Coating effect of $LiFePO_4$ and Al_2O_3 on $Li_{1.2}Mn_{0.54}Ni_{0.13}Co_{0.13}O_2$ cathode surface for lithium ion batteries

B. Seteni[a,b], N. Rapulenyane[a], J.C. Ngila[b], S. Mpelane[b], H. Luo[a*]

[a] *Council for Science and Industrial Research, Pretoria, South Africa*

[b] *University of Johannesburg, Johannesburg, South Africa*

**Corresponding author: Tel: +2712 841 2389; Fax: +2712 841 2135; Email: hluo@csir.co.za*

GRAPHICAL ABSTRACT

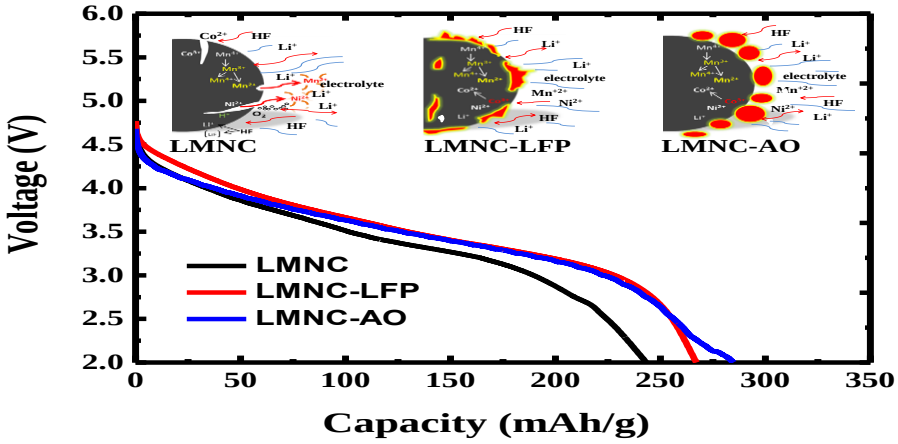

ABSTRACT

Lithium-manganese-rich cathode material $Li_{1.2}Mn_{0.54}Ni_{0.13}Co_{0.13}O_2$ is prepared by combustion method, and then coated with nano-sized $LiFePO_4$ and nano-sized Al_2O_3 particles via a wet chemical process. The as-prepared $Li_{1.2}Mn_{0.54}Ni_{0.13}Co_{0.13}O_2$, $LiFePO_4$-coated $Li_{1.2}Mn_{0.54}Ni_{0.13}Co_{0.13}O_2$ and Al_2O_3-coated $Li_{1.2}Mn_{0.54}Ni_{0.13}Co_{0.13}O_2$ are characterized by X-ray diffraction, scanning electron microscopy and transmission electron microscopy. The scanning electron microscopy shows the agglomeration of the materials and their nanoparticle size which ranges between 80 - 100 nm. The transmission electron microscopy confirmed that $LiFePO_4$ forms a rough mat-like surface and Al_2O_3 remain as islandic particles on the surface of the $Li_{1.2}Mn_{0.54}Ni_{0.13}Co_{0.13}O_2$ material. The $Li_{1.2}Mn_{0.54}Ni_{0.13}Co_{0.13}O_2$ coated with $LiFePO_4$ and $Li_{1.2}Mn_{0.54}Ni_{0.13}Co_{0.13}O_2$ coated with Al_2O_3 exhibits improved electrochemical performance. The initial discharge capacity is enhanced to 267 $mAhg^{-1}$ after the $LiFePO_4$ coating and 285 $mAhg^{-1}$ after the Al_2O_3 coating compared to the as-prepared $Li_{1.2}Mn_{0.54}Ni_{0.13}Co_{0.13}O_2$ material that had an initial discharge capacity of 243 $mAhg^{-1}$. Galvanostatic charge–discharge tests at 20 mAg^{-1} display longer activation of Li_2MnO_3 phase and higher capacity retention of 93% after 10 cycles for $Li_{1.2}Mn_{0.54}Ni_{0.13}Co_{0.13}O_2$-$LiFePO_4$ compared to $Li_{1.2}Mn_{0.54}Ni_{0.13}Co_{0.13}O_2$-$Al_2O_3$ of 88% after 10 cycle and LMNC of 83% after 10 cycles. Meanwhile $Li_{1.2}Mn_{0.54}Ni_{0.13}Co_{0.13}O_2$-$LiFePO_4$ also shows higher rate capability compared to $Li_{1.2}Mn_{0.54}Ni_{0.13}Co_{0.13}O_2$-$Al_2O_3$.

***Keywords*:** Lithium ion battery, $Li_{1.2}Mn_{0.54}Ni_{0.13}Co_{0.13}O_2$, Surface modification, Rate performance, Cyclability

1. Introduction

The commercially available cathode materials for lithium ion batteries such as layered $LiCoO_2$, spinel $LiMn_2O_4$ and olivine $LiFePO_4$ do not satisfy the requirements for plug-in hybrid-electric vehicles (PHEVs). This is mainly due to low discharge capacities and voltage ranges of 100 – 160 $mAhg^{-1}$and 2.0 – 4.2 V, respectively. These PHEVs generally require discharge capacities with rate profiles and greater power range that can at least meet a >64 km distance at minimal [1]. Due to that, globally much attention has been given to these materials in search of trying to improve their electrochemistry output. As much attention is given to the mentioned materials, a new and promising family of lithium-manganese-rich cathode (LRC) is emerging in the research space. These LRCs are reported to deliver superior practical discharge capacities of ~240 mAh/g between 2.0 – 4.8 V potential window when respective metal precursors are maneuvered to provide lithium-manganese rich oxide structure ($Li_{1+x}Mn_{1-x-y-z}Ni_yCo_zO_2$) [2]. However, also these LRCs do not meet the requirements for the ideal battery to power the PHEVs due to high affinities towards the electrolyte resulting to unstable structures hence low cyclability performances [3].

In the structure of these LRCs, in particular of $Li_{1+x}Mn_{1-x-y-z}Ni_yCo_zO_2$, the nearest-neighbor of the manganese and nickel ions have a tendency of adopting Mn^{4+} and Ni^{2+} chemical states and these ions are responsible for the stability and high voltages of the material structure, respectively [4-6]. Li^+ and Mn^{4+} ions are organized in localized regions to form a Li_2MnO_3-like structure which provides extra Li^+ ions that contributes to high discharge capacities [7]. These LRCs can also be represented as a two-component notation of $xLi_2MnO_3 \cdot (1-x)\ LiMO_2$ (where $0 < x < 1$ and M = Mn, Ni, Co) [8]. Thackeray and coworkers have been intensely engaged on investigating the electrochemical benefits of these LRCs materials especially those with elemental composition of $Li_{1.2}Mn_{0.6}Ni_{0.2}O_2$ and $Li_{1.2}Mn_{0.54}Ni_{0.13}Co_{0.13}O_2$. These in particular are reported to deliver discharge capacities of about 240 mAh/g with clear cut decrease on costs and toxicity because of low carcinogenic cobalt and high environmentally benign manganese contents [5-8]. However, a number of drawbacks impede the commercialization process of these oxides, such drawbacks include: (1) high irreversible capacity gap at first charge–discharge cycle; (2) poor rate performance; (3) poor cyclability (4) voltage decay due to structural distortion during long-term cycling [9-11].

Many efforts have been invested to solve these drawbacks, such as fabrication of nano-sized materials, optimized preparation methods, crystal-plane tuning and surface modification. Among these efforts, surface modification has been the most promising one in solving the mentioned problems due to its simplicity and effectiveness for LRCs [12]. Basically, this method forms a coating barrier on the surface of the active material. The formed barrier hinders and minimizes direct contact between the active particles and the electrolyte which can result to side reactions that can lead to the reduction/oxidation ($Mn^{4+} \rightarrow Mn^{3+}/Ni^{2+} \rightarrow Ni^{+4}$) of valuable metal ions. These undesired formed ions can disturb Li^+ ion migrations within the system and this may result in reduced capacities and cycling stabilities [13].

Phosphates [14-17], metal oxides, fluorides and carbon [12] are commonly used agents in the surface modification method [17-19]. Nonetheless, the electrochemical performance of the modified LRCs is still unsatisfactory mostly because of the disturbed Li^+ ion migrations routes during delithiation/lithiation processes and low ionic conductivity of the modified material's surface [20]. Usually in this method, the introduction of the modifying agent on the surface of the particle is achieved by solution chemistry to help in enhancing the conductivity of these modified LRCs and form very thin layers/barriers on their surface which will result in further more promising electrochemical outputs [21-24].

This method has been proven to have promising effects on the initial charge-discharge capacities with minimized voltage decay and enhanced rate performances [21, 25-28]. Different authors have reported on the surface modification of the $xLi_2MnO_3 \cdot (1-x)\ LiMO_2$ using olivine structured materials. On these

reports the improvement was greatly attributed to the Li_3PO_4-related structure which acted as a Li^+ ion conductor and as a protecting agent against the harsh electrolyte at a potential that is at least at 5V vs. Li^+. On these olivine surfaces, Kang and Thackeray further note that Ni^{2+} and Mn^{4+} which are responsible for high voltages and stability respectively, are the nearest ions at the Li_3PO_4/xLi_2MnO_3 (1-x) $LiMO_2$ to provide more stability at the electrode surface by suppressing the formation of Mn^{3+} ions which leads to the bleeding out of manganese from the formed particles. Additionally, Gallagher and co-workers submit that the olivine structured materials have much stronger bonds to the oxygen atoms compared to other oxides thus resulting stable and safe cathode materials [29]. On the other hand, alumina (Al_2O_3) also has been used to modify the surface of the xLi_2MnO_3 (1-x) $LiMO_2$ to improve the electrochemical output of the material. The benefits of aluminating the surface of these materials include: improved capacities due to the prevention of dissolution of metal ions by the harsh electrolyte resulting in stable cyclability. This of course is also due to the barrier formed on the surface. This barrier formed by the Al_2O_3 is able to keep more oxygen vacancies generated in the initial process which is greatly responsible for Li^+ ion intercalations with enhanced rate performances during charge and discharge processes as Zou and coworkers explain [30].

In this study, the as-prepared $Li_{1.2}Mn_{0.54}Ni_{0.13}Co_{0.13}O_2$ (LMNC) material was synthesized through a simple combustion method and coated by an easy one step process which resulted in improved electrochemical activities, then coated with electrochemically active nano-sized $LiFePO_4$ (LFP) and electrochemically inactive Al_2O_3 (AO) respectively. The three samples; as-prepared LMNC, LMNC-LFP and LMNC-AO were evaluated.

2. Experimental

2.1 Materials and synthesis route

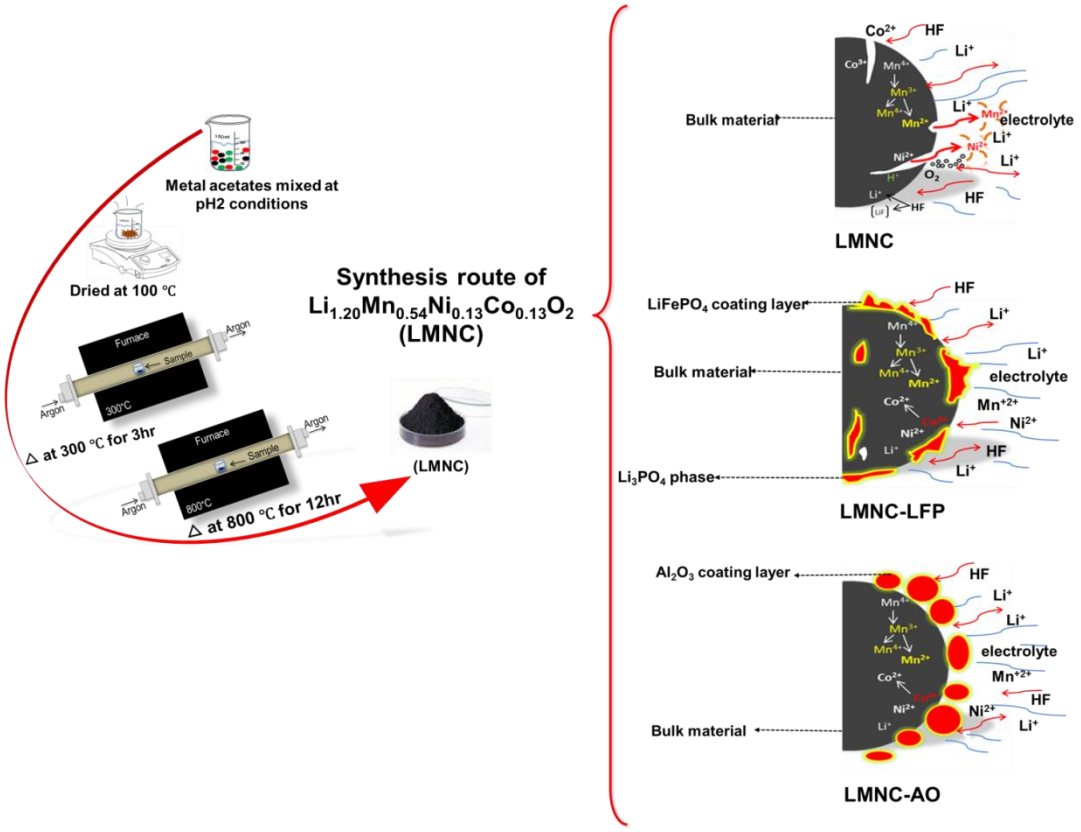

Scheme 1. Schematic diagram for the synthetic process of the LMNC coated with LFP and AO

All the reagents were analytical grade and purchased from Sigma Aldrich. The cathode materials were synthesized through the combustion method. Stoichiometric weights of the acetates Li-$(COOCH_3)_2{\cdot}2H_2O$, Mn-$(COOCH_3)_2{\cdot}4H_2O$, Ni-$(COOCH_3)_2{\cdot}4H_2O$ and Co-$(COOCH_3)_2{\cdot}4H_2O$ were used as precursor agents for the proposed system and measured out to obtain a standard batch size of five grams. This mixture of precursors was first dissolved in deionized water and then citric acid ($C_6H_8O_7$) was added as the chelating agent. The pH of the solution was adjusted to 2 using concentrated nitric acid (HNO_3). The mixture was continuously stirred for about 45 minutes at 80 °C for the formation of a homogeneous mixture of gel. Then the mixture was kept under a hot-plate for 2hrs at 100 °C to evaporate all the water from the obtained elemental composite. After the water was totally evaporated a black powder was formed which combusted to a fine brown powder. The powder blustered in an argon blow furnace at 300°C for 3 hours, subsequently calcined at 800 °C for 12 hours to ensure the formation of a proper phase for the crystalline structure. Amounts of 5g of the obtained material were suspended in 100ml ethanol in two different beakers, then, a nano-sized powder of 5 wt% $LiFePO_4$ and 5 wt% Al_2O_3 were added respectively and stirred for 1hr at 50 ℃. After the total evaporation of the ethanol the powders were blustered at 500℃ for three hours in an argon flowing furnace. The heating rate was 5℃/min. Finally, the material was collected from the furnace, grounded and stored in an Argon filled glove-box until was made into a cathode electrode.

2.2 Characterization techniques

For the morphology of the obtained powders a ZEISS ULTRA SS (Germany) field emission scanning electron microscope (FESEM) was used for the capturing of the images. The X-Max50mm^2 energy dispersive spectrometer (EDS) from the FESEM was also used to obtain information regarding the elements present in the samples. The bright field transmission electron microscopy (TEM) (JEOL JEM-2010F) coupled with an Oxford EDS detector was employed to evaluate the structure and composition of the nanoscale metal particles. X-ray diffraction (XRD) patterns were recorded by a Bruker AXS D8 ADVANCE X-ray Diffractometer with Ni-filtered Cu Kα (λ = 5406Å). The X-ray tube operating parameters were 40 kV and 40 mA. The measurements were taken with 2 Theta (2θ) angle ranging from 10 to 70°, with a scanning rate of 0.02/s with a dwell time of 5.0/s.

2.3 Cell assembling and measurements

The working electrodes were prepared from a paste by mixing 80 wt% of the prepared material, 10 wt% of the conductive acetylene black, and 10 wt% of the polyvinylidene fluoride binder in N-methyl-pyrrolidone (NMP) solvent. The paste was coated on the aluminum foil and then dried at 120 °C for 4 h under vacuum before the cell was assembled. The half-cells (coin-type CR2032) were assembled in an argon filled glove box (O_2<0.5ppm, H_2O<0.5ppm, Mbraun - Labstar mb-ox-SE1). The coin cell consisted of a metallic lithium foil anode, the prepared cathode electrode, a thin polypropylene membrane (Celgard 2300) as a separator and an electrolyte of 1 M $LiPF_6$ in a mixture of ethylene carbonate and dimethyl carbonate (1:1 volume ratio). The Galvanostatic charge/discharge tests were conducted on a multichannel Maccor (Series 4000) battery testing system at different current densities between 4.8V and 2V (vs Li/Li^+) at room temperature.

3. Results and discussion

3.1 Microscopic and spectroscopic characterization

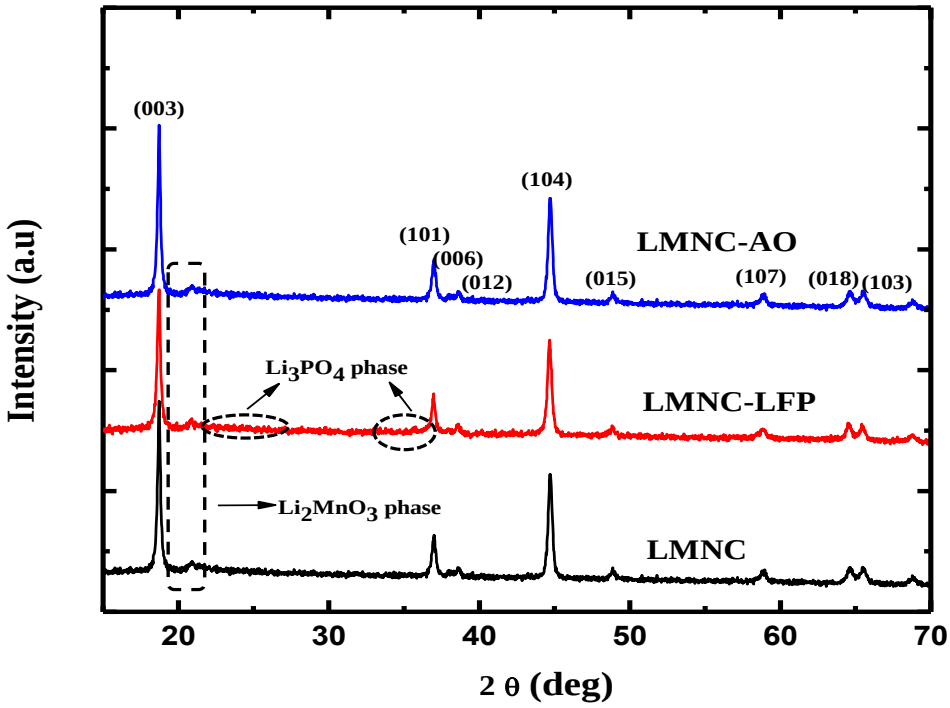

Fig. 1. XRD patterns: as-prepared LMNC, LMNC-LFP and LMNC-AO.

XRD patterns of LMNC, LMNC-LFP and LMNC-AO are shown in Fig. 1. The three samples are all indexed as layered rock-salt structures and hexagonal α-$NaFeO_2$-type with space group symmetry of R3*m*. To all the sample spectrums, weak peaks near 2θ = 20 - 23° indicates the presence of the super-lattice ordering of Li-rich and Mn material of monoclinic Li_2MnO_3 composition with a space group symmetry of *C2/m* [8, 31], as indicated by the dotted circles. The clear separation of (018/103) and (006/012) peaks indicate good crystallization degree of the samples [18, 20]. No additional/unindexed peaks are observed in all the samples and this indicates the absence of impurities. Nonetheless, in the LMNC-LFP there are some minor peaks which are indexed to the presence of Li_3PO_4-related phase from the olivine structure (in the square boxes) [20, 27]. However, in the LMNC-AO there are no extra peaks due to the amorphous structure and low content of the Al_2O_3 [7, 12, 32].

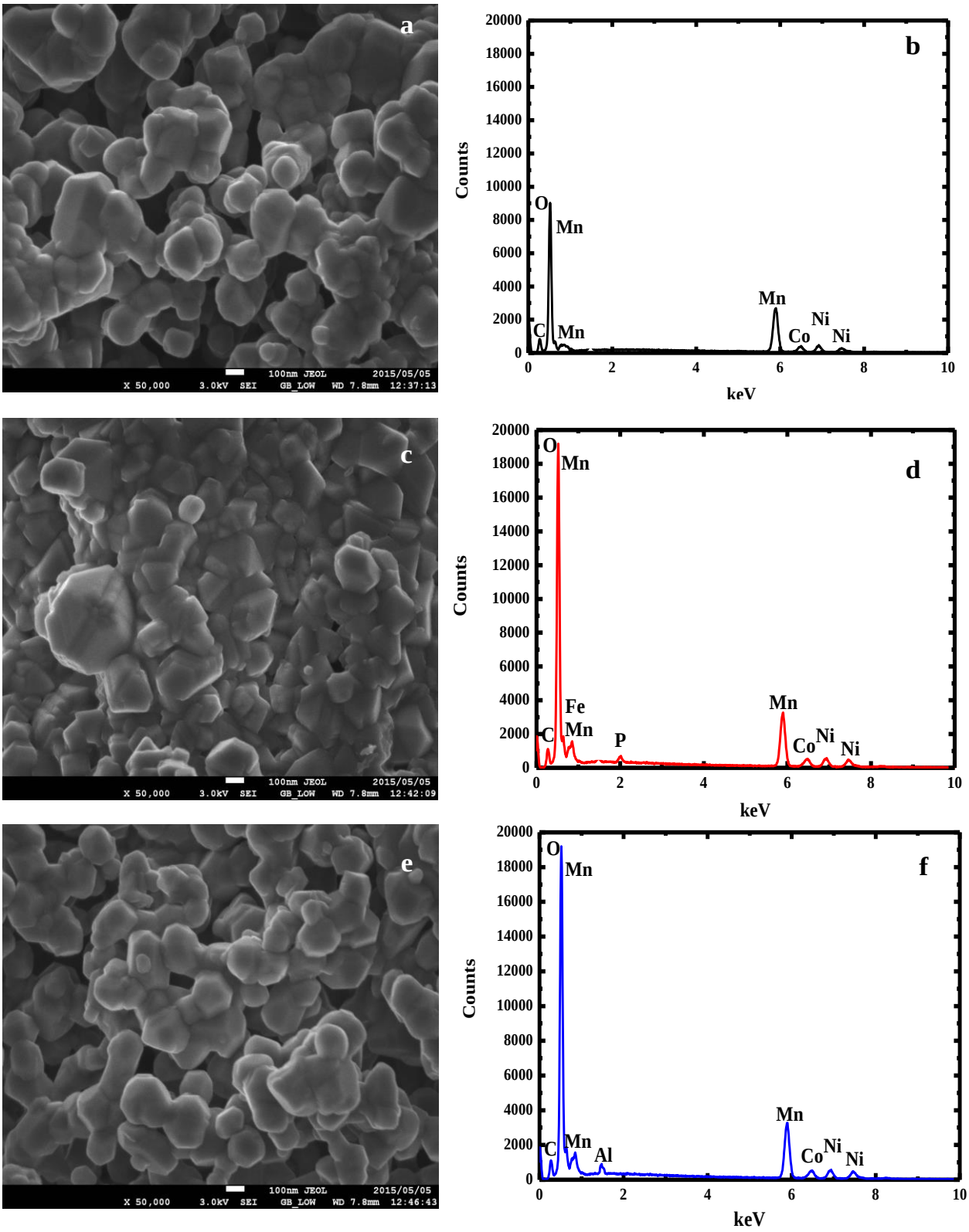

Fig. 2. SEM images and EDS spectra: as-prepared LMNC (a and b), LMNC-LFP (c and d) and LMNC-AO (e and f).

The morphologies of the samples were investigated by observing SEM images and the distribution/composition of the present elements in all the samples by electron diffraction spectroscopy EDS as shown in Fig.2. All the samples have high levels of agglomeration yet the SEM images of (a) and (e) are similar indicating less change after the coating by AO. However, after coating with LFP (c) the particle size appears to have decreased and more agglomerated compared to the (a) and (e). The EDS showed the distribution and the composition of the element of the samples. All the expected elements (Mn, Ni, Co, O, Fe, P and Al) in the samples were present except P in sample (c) and Al in sample (e) which both indicates a successful modification on the surface of the particles.

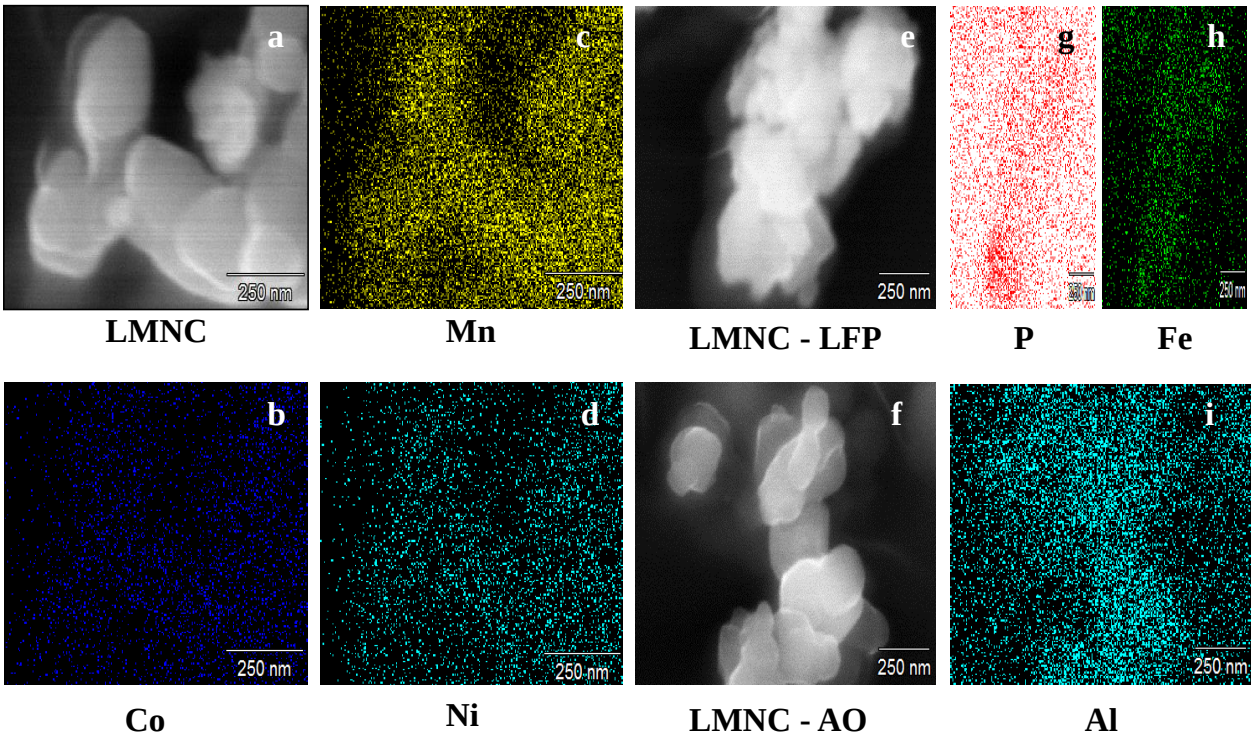

Fig. 3. EDS dot mappings: as-prepared LMNC (a, b, c and d), LMNC-LFP (e, g and h) and LMNC-AO (f and i).

Fig. 3 shows EDS dot mapping measurements which were taken from different areas of the samples compared to the SEM images in Fig. 2. This was done to further prove that the elements were evenly distributed in the samples. Fig.3 (a, b, c and d) present the prepared image of LMNC and its evenly distributed elements (Mn, Co and Ni). LMNC-LFP area (e) of the LFP-coated sample indicates the presence and distribution of P and Fe, (g) and (h) respectively. Fig. 3 (f) presents the AO-coated and showing the presence and the distribution of Al for the LMNC-AO (i).

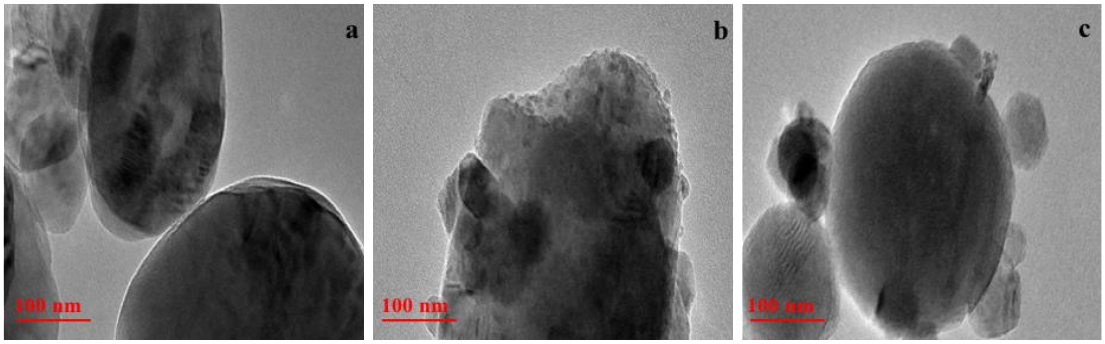

Fig. 4. TEM images: as-prepared LMNC (a), LMNC-LFP (b) and LMNC-AO (c).

For further microscopic scrutiny, TEM analysis was conducted to the respective samples and the results are shown in Fig. 4. The images show the bulk of the nanoparticles of the LMNC as prepared (a) and the coatings from both LMNC-LFP (b) and LMNC-AO (c). The as-prepared LMNC (a) has a clean and smooth surface grain edge compared to the coated LMNC-LFP (b) which has a rougher grain edge. Also at the LMNC-AO particle grain (c) the image reveals islandic particles situated on the surface of the material. These islandic particles at the LMNC-AO (c) surface results from the amorphous phase of the Al_2O_3 coated on the surface bulk particles.

3.2 Initial-second Galvanostatic curves and cycling performance of the as-prepared LMNC, LMNC-LFP and LMNC-AO.

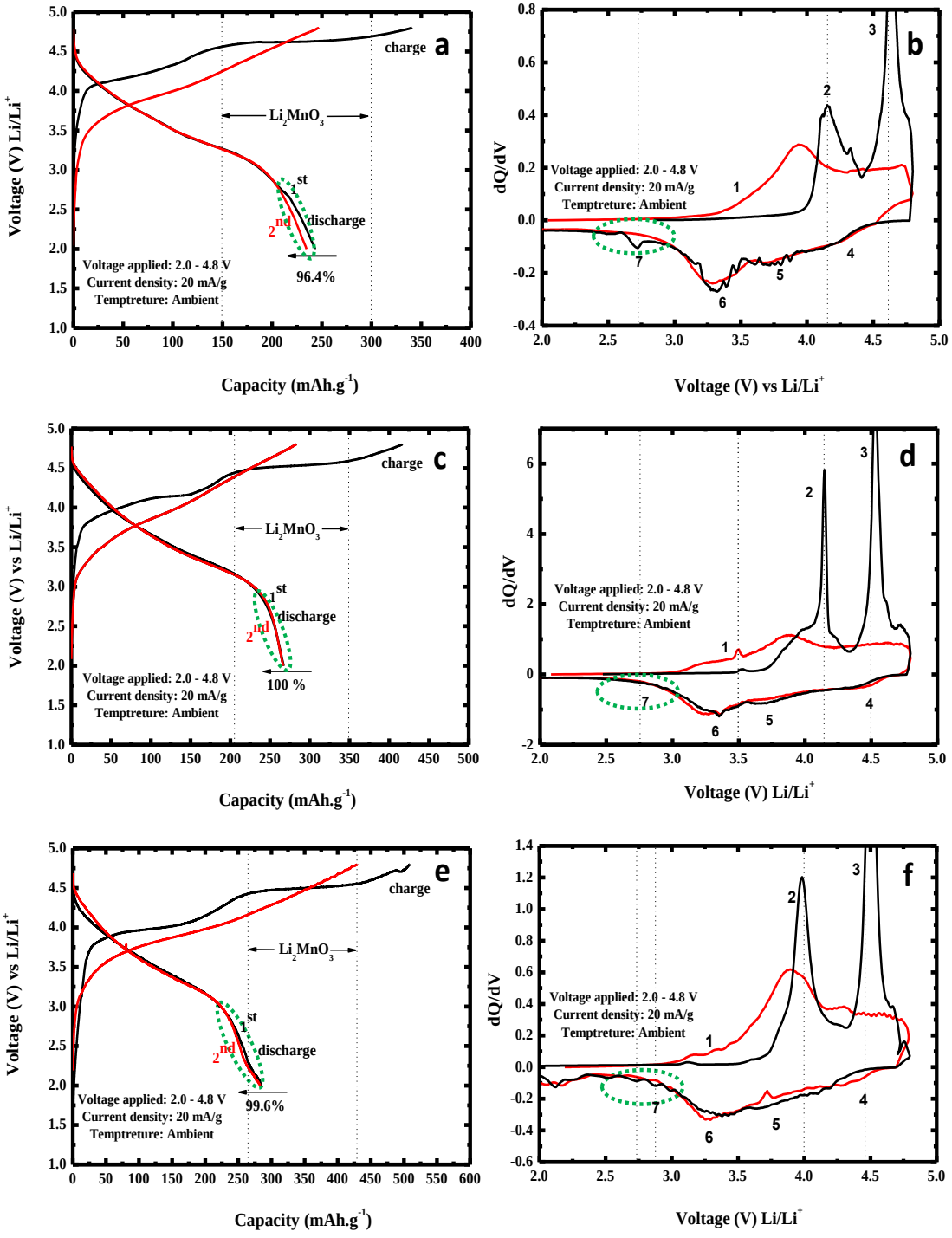

Fig.5. Initial-second Galvanostatic curves LMNC (a-b), LMNC-LFP (c-d) and LMNC-AO (e-f).

Fig. 5 shows the initial-second Galvanostatic properties of the as-prepared LMNC (5a), LMNC-LFP (5b) and LMNC-AO (c) within the voltage window of 2 V and 4.8 V at 20 mAg^{-1}. The three lithium-

manganese rich cathode materials yield different electrochemical characteristics which are greatly influence by the surface modifications in each material. First, the initial charge of the as-prepared LMNC has a plateau at slightly < 4.5 V [18]. The mechanism of this < 4.5 V plateau is reported to be complex and thus far assumed to be caused by the oxygen removal with a simultaneous delithiation and moving of transition metal ions from the surface to the actual bulk nanoparticles [31, 33]. The initial charge of the LMNC (5a) at this plateau yielded a charge capacity of 340 $mAhg^{-1}$ with the initial discharge capacity of 243 $mAhg^{-1}$ which can be quantified to 71% of the initial charge capacity. Secondly, the LMNC-LFP (5c) on the other hand yielded an initial charge capacity of 416 $mAhg^{-1}$ with the initial discharge capacity of 267 $mAhg^{-1}$ at a slightly > 4.5 V plateau. The LMNC-LFP initial discharge capacity is 63% of the initial charge capacity. Thirdly, the LMNC-AO (5e) yielded a charge capacity of 508 $mAhg^{-1}$ with the initial discharge capacity of 285 $mAhg^{-1}$ which is 51% of the LMNC-AO initial charge capacity at a slightly > 4.5 V. The three materials have voltage profiles that are within the 2.23 V and 4.5 V which are followed by the extraction of lithium and oxygen loss in the form of lithia (Li_2O) within the voltage window of 4.5 V and 4.8 V as represented by the two-notation equation (1) below [34]:

$$LiMO_2 \rightarrow Li^+ + MO_2 \,(2.23\ V - 4.5\ V)$$

$$Li_2MnO_3 \rightarrow 2Li^+ + 1/2O_2 + MnO_2 \,(4.5\ V - 4.8\ V) \qquad (1)$$

The irreversible capacity loss of the lithium-rich manganese materials has been reported to be complicated. Most researchers submit it is because of the synergistically integrated two layers: Li_2MnO_3-phase (C2/*m* space group symmetry) and $LiMO_2$-phase (R3*m* space group symmetry) (M = Mn, Ni or Co) as indicated by the XRD under Fig. 1. This irreversible capacity is due the irreparable loss of Li_2O during activation as expressed in equation 1.

The first discharge capacities of the LMNC, LMNC-LFP and LMNC-AO are 243 mAh/g, 267 $mAhg^{-1}$ and 285 $mAhg^{-1}$ respectively, which are with other published electrochemical performances as recently stated by other researchers [29, 34, 35]. However, it is worth noting that regardless the surface modifications of this lithium-manganese rich type materials the second discharge capacities usually decrease severely compared to the initial discharge [21]. This of course is greatly attributed by the metal ion layered composition and the method used to prepare the materials. In this study we used combustion method to prepare the LMNC, subsequently deposited the LFP and AO on the surface of the as-prepared LMNC. The second discharge capacity of the LMNC-LFP did not decrease nor was increase rather a 100% of the initial discharge 267 $mAhg^{-1}$ obtained. This is also observed in the LMNC-AO second discharge capacity which is 99.6% of the initial discharge capacity of 285 $mAhg^{-1}$. LMNC-LFP has a superior improvement in the second discharge capacities compared to the LMNC-AO and as-prepared LMNC second discharge capacity in which for the LMNC is 99.4% of the initial discharge capacity of 243 $mAhg^{-1}$[22].

3.3 Initial-second dQ/dV plots of the as-prepared LMNC, LMNC-LFP and LMNC-AO

For further electrochemical analysis of the initial and second charge-discharge cycles for the three samples: as-prepared LMNC (b), LMNC-LFP (d) and LMNC-AO (f), differential capacity versus voltage (dQ/dV) plots are illustrated in Fig.5. During the first charge cycle of the three samples, peak 2 at 4.1 V is observed. This peak is approved to be the oxidation of Ni^{2+} to Ni^{4+} and the peaks at ≤ 4.5 V (peak 3 in all samples) are attributed to the extraction of Li_2O from the Li_2MnO_3 component of the material [2, 34, 36]. It is noticed that this peak 2 at 4.1 V is much more prominent in sample LMNC-LFP (d) compared to others confirming a rapid oxidation of Ni^{2+} to Ni^{4+} hence the plateau of the Li_2MnO_3-activation is achieved at > 4.5 V for LMNC-LFP (d) compared to others. This phenomenal indicates that LMNC-LFP

(d) at 4.1V has more Ni^{4+} than Ni^{2+} in which the latter nickel ion is responsible for high voltages hence low voltages for this sample [37]. During the initial and second charge-discharge cycles of the materials, in the LMNC-LFP (d) and LMNC-AO (f) appears peak 1 at 3.5-3.6 V which is attributed to the reduction of Ni^{4+} via Ni^{3+} to Ni^{2+} and this peak is not observed for the as-prepared LMNC which means not much oxidation of Ni^{2+} to Ni^{4+} hence LMNC has high voltage plateau for the Li_2MnO_3-activation [38].

For the first charge cycle a projecting peak 3 above 4.5 V is observed in all the three samples. The LMNC-AO peak 3 during the charging process above 4.5 V (~4.7 V) appears to be more prominent compared to other samples. Of course, this attests the superior initial charge peak of the LMNC-AO observed in Fig. 5 (d). However, during the first discharge cycle, no reduction peak above 4.5 V is observed in all three samples and this confirms the irreversible capacity of the Li_2MnO_3 component of the sample materials. During the second cycle in all three samples, the main peak 2 at 4.1 V appears to shift to 3.9 V indicating that some modification took place either in the bulk material or in the electrolyte interface after the first cycle. Peak 2 shifts from 4.1 V to 3.8 V during the initial and second charge cycles of the three materials, however LMNC-AO both peaks for the two cycles is much more projected than other samples. This peak is reported to be relative with lithium metal-ion intercalation and reduction of both nickel and cobalt metal ions in the materials. Also, this peak 2 is assumed to be linked with lithium metal ion situated at the tetrahedral and octahedral positions of the material's crystal lattice [25, 39-41]. In the initial discharge cycles of as-prepared LMNC (b) and LMNC-AO (d) there peak 7 which appears to be weak at 2.8 V. This peak is indexed to the spinel phase of MnO_2 component formed in the first charge during lithium ion metal intercalation. The peak is also reported to indicate the phase transformation from layered structure to spinel structure which can increase the initial coulombic efficiency [42]. Also, this peak indicates a reduction process of Mn^{4+} to Mn^{3+} during the first discharge in which this process leads to structural alteration from layered oxide to a spinel oxide. However, in the LMNC-LFP (d), there is no small peak 7 appearing at about 2.8 V which means the LFP deposited on the surface of the as-prepared LMNC (a) retained the Mn^{4+} and no reduction of this tetravalent ion to Mn^{3+} and no structural alteration from layered oxide to spinel hence a 100% discharge capacity was obtained by the LMNC-LFP (d). In a nutshell, the LMNC-LFP (d) remained superior to both the as-prepared LMNC (a) and LMNC-AO (c) when it comes to minimizing or eliminating the structural formation of the layered oxide to spinel-like oxide in the first and second discharge cycles. These results of the LMNC-LFP (d) suggest that the LFP might be the better surface modifying agent that can be used for increasing discharge capacity of the LMNC still be able to minimize the contact between the bulk material and the harsh electrolyte which usually result in the reduction of Mn^{4+} via Mn^{3+} to Mn^{2+} which leads to the dissolution of the metal-ions.

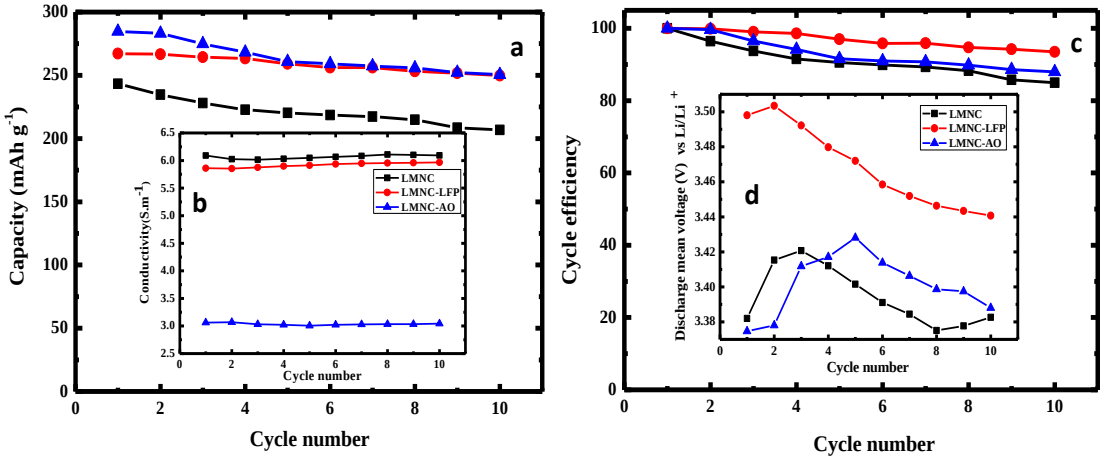

Fig.6. Capacity vs. cycle number (a), continuous conductivity (b) cycle efficiency vs. cycle number (c), discharge mean voltage (d) of the as-prepared LMNC, LMNC-LFP and LMNC-AO.

Fig.6 shows the cycle performance of the as-prepared LMNC, LMNC-LFP and LMNC-AO. As observed in Fig.6 (a), the as-prepared yields a rapid capacity fade and its capacity decreases down to 206 $mAhg^{-1}$ after 10 cycles and only about 85% of its initial discharge capacity is obtained. However, the LMNC-LFP discharge capacity after 10 cycles is 250 $mAhg^{-1}$ and corresponds to the 94% of its initial discharge capacity. The LMNC-AO on the other hand, yields a discharge capacity of 251 mAh/g discharge capacity 10 cycles and this capacity is 88% of its initial discharge capacity. These results advocate that the LFP modification on the surface of the as-prepared LMNC can significantly stabilize its cycling performance. In Fig.6 (c), we compared the cycling efficiency of the as-prepared LMNC, LMNC-LFP and LMNC-AO electrodes using the results obtained at 20 mAg^{-1} in Fig.6 (a). The LMNC-LFP and LMNC-AO electrode cycles had higher efficiency, with averages close to 96% and 89% of their initial discharge capacities. However, the as-prepared LMNC electrode decreases towards 85% on cycling as the surface is destabilized by the speculated side reactions resulting from the contact with the electrolyte at 4.6 V. During this 10 cycle performance, the as-prepared LMNC electrode capacity drops, this drop in capacity was anticipated due Li^+ ion diffusion at the electrode's surface and this was due to the side reactions between the electrode and the electrolyte [29]. Thus far, the chemistry of the LFP and its mechanisms at the surface of the as-prepared LMNC has not yet been founded and proved beyond reasonable doubt [22, 29], nonetheless the obtained electrochemical data suggest that it provides not only effectual protective layer at high voltages of ~4.8 V but also as a first-rate Li^+ ion conductor observed. Using the MACCOR battery tester, Fig. 6(b) further proves this point, as observed the conductivity of the LMNC-LFP is more superior to that of the AO and we assume this is due to the olivine-$LiFePO_4$ defect which is the Li_3PO_4 structure. Kang and co-workers advances this submission by stating that $Li_{3-x}M_{x/2}PO_4$ ((M = Fe, Mn, Ni) $(0 < x < 1)$) is greatly accountable for the enhanced electrochemistry of the olivined-LMNC surface hence LMNC-LFP provide higher conductivity than LMNC-AO [29]. These results may offer other prospects and future outlook for designing lithium-ion conducting structures for stabilizing delithiated lithium-manganese rich oxide electrode surfaces using cheaper and effectual agent like LFP at high voltages. Additionally, Fig.6 (d) highlights one of the major challenges the lithium-manganese rich materials tend to have, the voltage decay challenge, which is usually caused by structural changes during charge and discharge processes. In this study the "discharge mean voltage' results were also acquired by MACCOR battery tester and used as a determining factor to reveal voltage decay during discharge processes. Thus, we have studied the voltage decay of the as-prepared LMNC, LMNC-LFP and LMNC-AO upon 10 cycles and results are shown in Fig. 6 (d). As observed, the three materials do not severely suffer much from voltage decay; possibly, this is due to the effectiveness of the combustion method used as the synthesis route. The method encouraged the formation of the super-lattice ordering of Li-rich and Mn material of monoclinic Li_2MnO_3 composition, which its fragment (MnO_2) remains greatly responsible for the structural stability throughout the charge and discharging processes after the initial cycles. Nonetheless, comparing the as–prepared LMNC and LMNC-AO both show greater fluctuation in voltage decay whereas, the LMNC-LFP had minor increment on voltage fade.

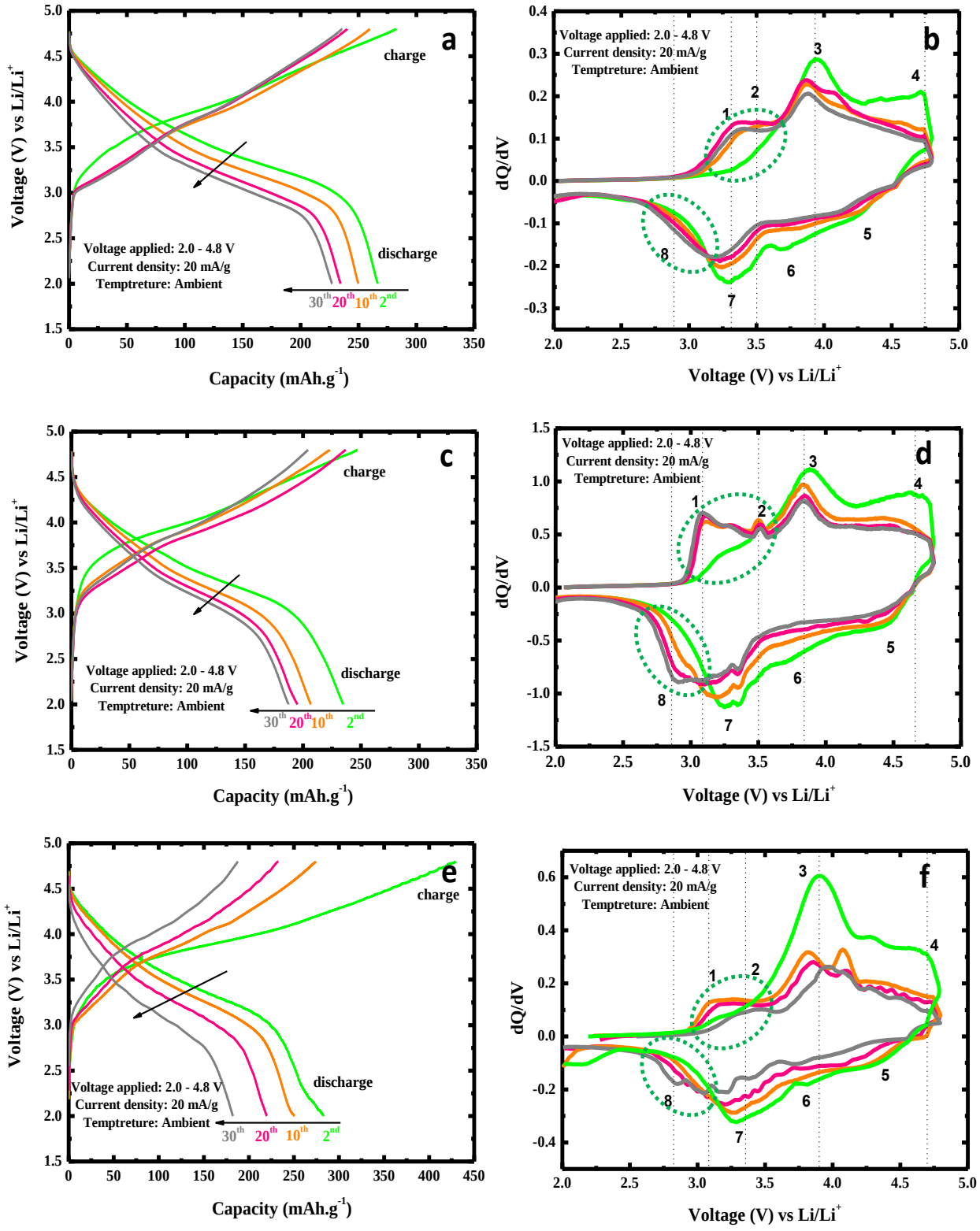

Fig.7. Charge-discharge capacities and parallel dQ/dV profiles of as-prepared LMNC (a-b), LMNC-LFP (c-d) and LMNC-AO (e-f) over the progression of 2 - 30 cycles at 20mA/g.

Following, we examined the corresponding dQ/dV of the as-prepared LMNC (a), LMNC-LFP (b) and LMNC-AO (c) and compared their structural changes as they undergone 2nd, 10th, 20th and 30th repetitive charge-discharge cycles at 20 mAg^{-1} as shown in Fig.7. It has been reported that the peaks over the voltage of 3.6 V are corresponding to the reduction and oxidation of Ni^{2+}/Ni^{4+} and Co^{3+}/Co^{4+}. At about 3.3 – 3.5 V after the activation of Li_2MnO_3 component through the liberation of Li_2O, occurs the reduction of Mn^{4+}/Mn^{3+} in the remaining MnO_2 as shown in equation 1 [20]. In Fig.7 the peaks after the 2nd cycle appear to shift to lower voltages at oxidation peaks and shift to lower reduction peaks as the cycles are prolonged. This indicates a smaller degree of polarization in the structures as the cycles are continued to the 30th. The area under curve for the LMNC-LFP (b) is much bigger compared those of as-prepared LMNC (a) and LMNC-AO (c) and this is consistent with its good capacity retention. During the 2nd cycle for all the three samples, a weak almost distinct reduction peak 1 (3.3 V) is observed. As the cycles are prolonged, peak 1 intensifies in all the samples corresponding to the oxidation peak 8 (2.8 V) which also appear to be intensifying. Peak 8 relates to the spinel-like phase of $LiMnO_2$. This occurrence is consistent with the mechanism proposed by Song et al., and other research groups. They state that the occurrence is due to phase transformation which is caused by the migration of transition metal ions from the transition metal layer to the lithium layer during cycling [43-47]. As the cycles are prolonged from the 2nd to the 30th, peak 8 in all the samples increases but LMNC-LFP (b) appear to be much stronger that the others. In the LMNC-LFP (b), there appears a new reduction peak 2 V at 3.5 V and this peak 2 is absent in the as-prepared LMNC and LMNC-AO indicates a diminutive layered MnO_2-phase that is left after the 30th cycle [20]. In all the three samples, the reduction peak 1 remains stronger than the oxidation peak 8 as the cycles are prolonged, and these two peaks for LMNC-LFP (b) appear to be stronger than the as-prepared LMNC and LMNC-AO. These results signify that the LFP coating possibly rapidly promotes the phase transformation of MnO_2 to spinel-like phase after the 2nd cycle. This transformation is associated with the larger amount of O_2^- ions supplied by the $FePO_4^-$ which result in more stable layered surface. Indeed, this pattern in the reduction peak 1 and oxidation peak 8 is evident in LMNC-AO (c), suggesting that the amount of O_2^- ions dictates the phase transformation of MnO_2 to spinel-like phase since LMNC-AO (c) (Al_2O_3) has lesser O_2^- ion than LMNC-LFP (b) ($LiFePO_4$). Some researchers consider phase transformation a problem that usually cause capacity fade, however, some researchers consider this transformation to be a framework structure which provides more stable cyclability [45, 48, 49]. One of the major drawbacks with spinel-like formation is that it decreases the average discharge voltage as can be seen in Fig.6 (d) and in Fig 5 (b), (d) and (f) and this is reported in the literature. This decrease in average discharge voltage usually leads to hysteresis during cycling and lower power densities. Also during discharging processes, cathodic peak 5 (4.5 V), peak 6 (3.8 V) and peak 7 (3.25 V) are observed. Peak 5 and peak 6 are an outcome of $Ni^{2+} \rightarrow Ni^{4+}$ with a possibility of oxygen reduction [38, 50-53]. Peak 7 in the three samples is observed and associated by Liu with the combination of $Mn^{4+} \rightarrow Mn^{3+}$ and accompanied by the oxygen reduction which results from the Li-ion insertion back into the bulk structure as reported by different authors [8, 33, 51, 54].

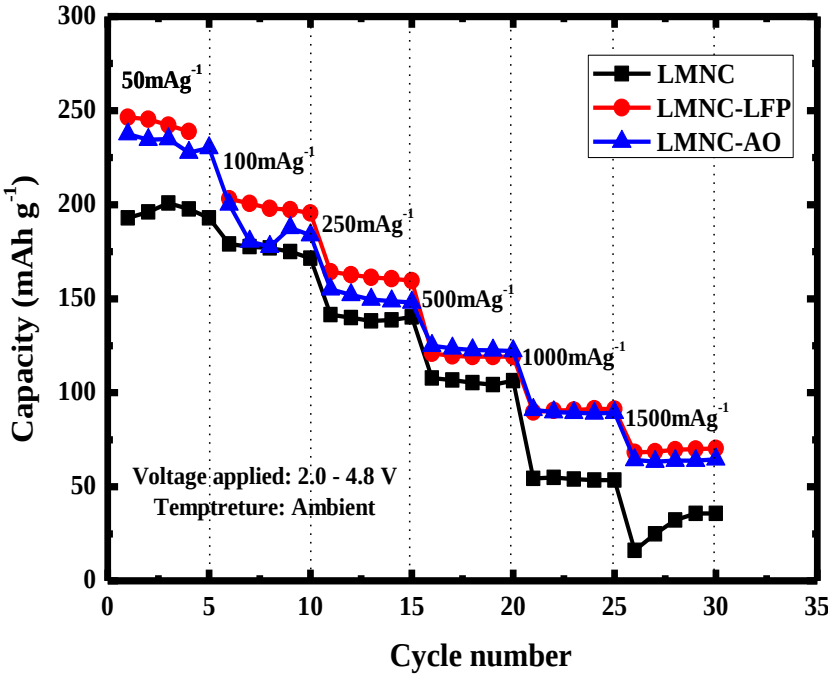

Fig.8. Cyclic performance of the as-prepared LMNC, LMNC-LFP and LMNC-AO at different discharge rates.

Fig.8 shows cyclic performance of the as-prepared LMNC, LMNC-LFP and LMNC-AO at different current densities at ambient conditions. The cells were charged from 2.0 V to 4.8 V and then for each 5 cycle they were discharged at different current densities, which are; 50 mAg^{-1}, 100 mAg^{-1}, 250 mAg^{-1}, 500 mAg^{-1}, 1000 $mAg^{-1}$and 1500 mAg^{-1}. The discharge capacities of the as-prepare LMNC decrease vividly as the current densities are increased and this attest that it suffers dismally from poor rate capability. Moreover, at 1500 mAg^{-1} the discharge capacity of the LMNC seem to increase from 0 $mAhg^{-1}$ to 49 $mAhg^{-1}$. These results prove that the as-prepared LMNC electrodes can be significantly damaged at high current densities. However, the LMNC-LFP and LMNC-AO both samples show a decent cyclic performance as the current densities are increased. This proves that indeed the LMNC surface modifications by LFP and AO can enhance the cyclic performance. Although both LFP and AO improves cyclic performance at high rates, LFP however remains slightly superior than AO as can be observed at 50 mAg^{-1} and 1500 mAg^{-1} the discharge capacities of LMNC-LFP are 249 $mAhg^{-1}$ and 75 $mAhg^{-1}$ respectively. Also the LFP remains a better choice than AO as modifying agent not only because it's better rate performance but also due to its cost effectiveness.

4. Conclusion

The present paper investigates the effect of the electrochemically active $LiFePO_4$ and the electrochemically inactive Al_2O_3 coated on the surface of the lithium-manganese rich $Li_{1.2}Mn_{0.54}Ni_{0.13}Co_{0.13}O_2$. By employing the combustion method and wet chemistry, crystalline and amorphous structures of $LiFePO_4$ and Al_2O_3, respectively were obtained on the surface of the as-prepared sample. Compared with the as-prepared $Li_{1.2}Mn_{0.54}Ni_{0.13}Co_{0.13}O_2$, both $LiFePO_4$ and Al_2O_3 modified surfaces showed improved electrochemical performances. From the obvious initial charge-discharge processes of the modified samples to their rate performances, both the modified samples compared to the as-prepared showed significant improvements. Nonetheless, $LiFePO_4$-modified remained superior to

Al_2O_3 in cyclic performances, voltage decay and rate performances. Indeed, the results prove that $LiFePO_4$ is a better surface modifying agent than Al_2O_3 and cost effective.

Acknowledgements

The authors acknowledge NRF/DST for funding the project, CSIR for providing the working space and the University of Johannesburg for the limitless access to the instruments.

References

[1] J.R.D. Z. Lu, Journal of The Electrochemical Society, 149 (2002) A815-A822.
[2] M. Armand, J.M. Tarascon, Nature, 451 (2008) 652-657.
[3] B. Scrosati, J. Garche, Journal of Power Sources, 195 (2010) 2419-2430.
[4] B. Dunn, H. Kamath, J.M. Tarascon, Science, 334 (2011) 928-935.
[5] J.B. Goodenough, Y. Kim, Chemistry of Materials, 22 (2009) 587-603.
[6] W.S. Yoon, S. Iannopollo, C.P. Grey, D. Carlier, J. Gorman, J. Reed, G. Ceder, Electrochemical and Solid-State Letters, 7 (2004) A167-A171.
[7] M.M. Thackeray, S.H. Kang, C.S. Johnson, J.T. Vaughey, S.A. Hackney, Electrochemistry Communications, 8 (2006) 1531-1538.
[8] A.R. Armstrong, M. Holzapfel, P. Novák, C.S. Johnson, S.H. Kang, M.M. Thackeray, P.G. Bruce, Journal of the American Chemical Society, 128 (2006) 8694-8698.
[9] J. Kikkawa, T. Akita, M. Tabuchi, K. Tatsumi, M. Kohyama, Journal of The Electrochemical Society, 158 (2011) A760-A768.
[10] N. Yabuuchi, K. Yoshii, S.T. Myung, I. Nakai, S. Komaba, Journal of the American Chemical Society, 133 (2011) 4404-4419.
[11] Y. Wu, A. Manthiram, Solid State Ionics, 180 (2009) 50-56.
[12] H. Li, H. Zhou, Chemical Communications, 48 (2012) 1201-1217.
[13] J. Liu, A. Manthiram, Journal of Materials Chemistry, 20 (2010) 3961-3967.
[14] J. Liu, A. Manthiram, Journal of Materials Chemistry, 20 (2010) 3961-3967.
[15] W.C. West, J. Soler, M.C. Smart, B.V. Ratnakumar, S. Firdosy, V. Ravi, M.S. Anderson, J. Hrbacek, E.S. Lee, A. Manthiram, Journal of the Electrochemical Society, 158 (2011) A883-A889.
[16] S.J. Shi, J.P. Tu, Y.Y.Tang, X.Y. Liu, Y.Q. Zhang, X.L. Wang, C.D. Gu, Electrochimica Acta, 88 (2013) 671-679.
[17] S.J. Shi, J. J.P. Tu, Zhang, Y.D. Zhang, X.Y. Zhao, X.L. Wang, C.D. Gu, Electrochimica Acta, 108 (2013) 441-448.
[18] Y.K. Sun, M.J. Lee, C.S. Yoon, J. Hassoun, K. Amine, B. Scrosati, Advanced Materials, 24 (2012) 1192-1196.
[19] X. Liu, J. Liu, T. Huang, A. Yu, Electrochimica Acta, 109 (2013) 52-58.
[20] Z. Wang, E. Liu, C. He, C. Shi, J. Li, N. Zhao, Journal of Power Sources, 236 (2013) 25-32.
[21] B. Liu, Q. Zhang, S. He, Y. Sato, J. Zheng, D. Li, Electrochimica acta, 56 (2011) 6748-6751.
[22] F. Wu, N. Li, Y. Su, H. Shou, L. Bao, W. Yang, L. Zhang, R. An, S. Chen, Advanced materials, 25 (2013) 3722-3726.
[23] B. Song, H. Liu, Z. Liu, P. Xiao, M.O. Lai, L. Lu, Scientific reports, 3 (2013).
[24] X. Liu, Q. Su, C. Zhang, T. Huang, A. Yu, ACS Sustainable Chemistry & Engineering, 4 (2015) 255-263.
[25] J.Y. Shi, C.-W. Yi, K. Kim, Journal of Power Sources, 195 (2010) 6860-6866.

[26] F. Wu, X. Zhang, T. Zhao, L. Li, M. Xie, R. Chen, ACS applied materials & interfaces, 7 (2015) 3773-3781.
[27] K.G. Gallagher, S.-H. Kang, S.U. Park, S.Y. Han, Journal of Power Sources, 196 (2011) 9702-9707.
[28] S.H. Kang, M.M. Thackeray, Electrochemistry Communications, 11 (2009) 748-751.
[29] J.F. Whitacre, K. Zaghib, W.C. West, B.V. Ratnakumar, Journal of Power Sources, 177 (2008) 528-536.
[30] G. Zou, X. Yang, X. Wang, L. Ge, H. Shu, Y. Bai, C. Wu, H. Guo, L. Hu, X. Yi, Journal of Solid State Electrochemistry, 18 (2014) 1789-1797.
[31] Z. Lu, J.R. Dahn, Journal of The Electrochemical Society, 149 (2002) A815-A822.
[32] M.M. Thackeray, S.H. Kang, C.S. Johnson, J.T. Vaughey, R. Benedek, S.A. Hackney, Journal of Materials Chemistry, 17 (2007) 3112-3125.
[33] C.J. Jafta, K.I. Ozoemena, M.K. M.K. Mathe, W.D. Roos, Electrochimica Acta, 85 (2012) 411-422.
[34] H. Liu, D. Qian, M.G. Verde, M. Zhang, L. Baggetto, K. An, Y. Chen, K.J. Carroll, D. Lau, M. Chi, ACS applied materials & interfaces, 7 (2015) 19189-19200.
[35] J. Li, Li. Wang, L. Wang, J. Luo, J. Gao, J. Li, J. Wang, X. He, G. Tian, S. Fan, Journal of Power Sources, 244 (2013) 652-657.
[36] M. Tabuchi, H. Shigemura, K. Ado, H. Kobayashi, H. Sakaebe, H. Kageyama, R. Kanno, Journal of power sources, 97 (2001) 415-419.
[37] W. Zheng, X. Xu, L. Cheng, M. Shui, J. Shu, S. Gao, Z. Lu, L. Feng, Y. Ren, Ionics, 19 (2013) 1509-1514.
[38] C.S Johnson, N. Li, C. Lefief, J.T. Vaughey, M.M. Thackeray, Chemistry of Materials, 20 (2008) 6095-6106.
[39] J. Bréger, Y.S. Meng, Y. Hinuma, S. Kumar, K. Kang, Y. Shao-Horn, G. Ceder, C.P. Grey, Chemistry of Materials, 18 (2006) 4768-4781.
[40] H.H. Li, N. Yabuuchi, Y.S. Meng, S. Kumar, J. Breger, C.P. Grey, Y. Shao-Horn, Chemistry of materials, 19 (2007) 2551-2565.
[41] S.H. Kang, C.S. Johnson, J.T. Vaughey, K. Amine, M.M. Thackeray, Journal of The Electrochemical Society, 153 (2006) A1186-A1192.
[42] K.J. Carroll, D. Qian, C. Fell, S. Calvin, G.M. Veith, M. Chi, L. Baggetto, Y. S. Meng, Physical Chemistry Chemical Physics, 15 (2013) 11128-11138.
[43] B. Song, Z. Liu, M.O. Lai, L. Lu, Physical Chemistry Chemical Physics, 14 (2012) 12875-12883.
[44] J.R. Croy, D. Kim, M. Balasubramanian, K. Gallagher, S.H. Kang, M.M. Thackeray, Journal of The Electrochemical Society, 159 (2012) A781-A790.
[45] K. Ito, K. Shoda, Y. Sato, M. Hatano, H. Horie, Y. Ohsawa, Journal of Power Sources, 196 (2011) 4785-4790.
[46] M. Gu, I. Belharouak, J. Zheng, H. Wu, J. Xiao, A. Genc, K. Amine, S. Thevuthasan, D.R. Baer, J.R. Zhang, ACS nano, 7 (2012) 760-767.
[47] Y.K. Sun, M.J. Lee, C.S. Yoon, J. Hassoun, K. Amine, B. Scrosati, Advanced Materials, 24 (2012) 1192-1196.
[48] G.R. Li, X. Feng, Y. Ding, S.H. Ye, X.P. Gao, Electrochimica Acta, 78 (2012) 308-315.
[49] Y. Li, M. Bettge, B. Polzin, Y. Zhu, M. Balasubramanian, D.P. Abraham, Journal of The Electrochemical Society, 160 (2013) A3006-A3019.
[50] S. Hy, F. Felix, J. Rick, W.N Su, B.J. Hwang, Journal of the American Chemical Society, 136 (2014) 999-1007.
[51] H. Koga, L. Croguennec, M. Ménétrier, P. Mannessiez, F. Weill, C. Delmas, Journal of Power Sources, 236 (2013) 250-258.
[52] N. Yabuuchi, K. Yoshii, S. T. Myung, I. Nakai, S. Komaba, Journal of the American Chemical Society, 133 (2011) 4404-4419.
[53] S. Hy, J.H. Cheng, J.Y. Liu, C.J. Pan, J. Rick, J.F. Lee, J.M. Chen, B.J. Hwang, Chemistry of Materials, 26 (2014) 6919-6927.
[54] J.H. Kim, C.W. Park, Y.K. Sun, Solid State Ionics, 164 (2003) 43-49.